Hypoxia In The Lower St. Lawrence Estuary: How Physics Controls Spatial Patterns

S. Lefort, Y. Gratton, A. Mucci, I. Dadou, D. Gilbert

Hypoxia in the Lower St. Lawrence Estuary: How physics controls spatial patterns

S. Lefort,[1] Y. Gratton,[2] A. Mucci,[1] I. Dadou,[3] and D. Gilbert[4]

Received 10 November 2011; revised 21 April 2012; accepted 31 May 2012; published 25 July 2012.

[1] A laterally integrated advection-diffusion two-dimensional model was implemented to simulate the spatial distribution of dissolved oxygen and the development of hypoxic conditions in the deep waters of the Laurentian Channel (Estuary and Gulf of St. Lawrence, Eastern Canada). Our simulations reveal that the horizontal distribution of dissolved oxygen in the bottom waters of the Laurentian Channel is determined by a combination of physical and biogeochemical processes, whereas its vertical distribution is governed by the deep water circulation. This result strongly suggests that the physics of the system and the source water properties are mostly responsible for the generation of a mid-water column oxygen minimum and the oxygen distribution pattern in the deep water column.

Citation: Lefort, S., Y. Gratton, A. Mucci, I. Dadou, and D. Gilbert (2012), Hypoxia in the Lower St. Lawrence Estuary: How physics controls spatial patterns, *J. Geophys. Res.*, *117*, C07018, doi:10.1029/2011JC007751.

1. Introduction

[2] Hypoxia ($[O_2] < 62.5\ \mu mol\ L^{-1}$) results from complex interactions between physical and biogeochemical processes [*Peña et al.*, 2010]. In coastal environments, eutrophication is often identified as the main cause of hypoxia. Nutrient discharge by rivers sustains high surface water primary production which, in turn, is exported to deep waters and serves as a sink for dissolved oxygen [*Cloern*, 2001]. Nevertheless, physical conditions limiting water ventilation (e.g., stratification) or remote advection of oxygen-poor water under a persistent pycnocline are also necessary for the development of hypoxia [*Diaz and Breitburg*, 2009]. Hypoxic conditions are reported in numerous fjords (e.g., Framvaren Fjord, Saanich Inlet) and semi-enclosed seas (e.g., Baltic Sea) where persistent stratification prevents the ventilation of deep waters [*Özsoy and Ünlüata*, 1997]. Given the global spread of hypoxia and its impacts in coastal ecosystems [*Diaz*, 2001; *Gilbert et al.*, 2010], we need to understand processes controlling hypoxic conditions, especially the relative contribution of physical and biogeochemical processes that regulate the development of hypoxic bottom waters.

[3] The deep waters (>250 m) of the Lower St. Lawrence Estuary (LSLE) (Figure 1) have been hypoxic since the mid-1980s [*Gilbert et al.*, 2005]. The bathymetry of the LSLE is marked by the presence of a deep channel, the Laurentian Channel, that extends from Tadoussac to the edge of the eastern Canadian continental shelf. The persistence of hypoxic conditions in the LSLE results from the year-round stratification of the water column and the estuarine circulation pattern. Throughout most of the year, the water column in the Laurentian Channel is characterized by three distinct layers [*Dickie and Trites*, 1983]: (1) a 25–50 m deep surface layer of low salinity (27–32) flowing seaward, (2) a 50 to 100 m thick intermediate layer of cold (−1 to 2°C) and saline (31.5–33) water flowing landward from the western Gulf [*Saucier et al.*, 2003], and (3) a deep layer that extends to depths of 350 m or more with warmer (4–6°C) and saltier (34–34.6) water flowing landward. The surface layer displays large seasonal variations in temperature and salinity due to atmospheric and buoyancy forcing. In winter, as tributary flow decreases and ice is formed, this layer becomes progressively colder and denser until it merges with the cold intermediate layer (CIL) [*Galbraith*, 2006; *Gilbert and Pettigrew*, 1997]. The CIL is separated from the bottom waters by a permanent pycnocline that inhibits the ventilation of deep waters [*Bugden*, 1991; *Craig and Gilbert*, 2008; *Tee*, 1989]. The deep waters originate from the edge of the continental shelf, enter the Gulf through Cabot Strait and travel landward to Tadoussac (Figure 1) where they are tidally upwelled due to an abrupt change in bathymetry (from 350 to ∼35 m) [*Gratton et al.*, 1988]. They are a mixture of cold and oxygen-rich Labrador Current Water (LCW) and warm oxygen-poor North Atlantic Central Water (NACW) whose proportions vary on a decadal or secular time scales [*Bugden*, 1991; *Gilbert et al.*, 2005]. Given that the bottom waters are isolated from the surface waters and atmosphere by a permanent pycnocline, dissolved oxygen in the bottom waters

[1]GEOTOP and Department of Earth and Planetary Sciences, McGill University, Montreal, Quebec, Canada.
[2]Institut National de la Recherche Scientifique, Eau Terre et Environnement, Quebec, Quebec, Canada.
[3]Laboratoire d'Etudes en Géophysique et Océanographie Spatiales, UMR5566/CNRS/UPS, Toulouse, France.
[4]Maurice Lamontagne Institute, Fisheries and Oceans Canada, Mont-Joli, Quebec, Canada.

Corresponding author: S. Lefort, Department of Earth and Planetary Sciences, McGill University, 3450 University St., Montréal, QC H3A 2A7, Canada. (stelly.lefort@gmail.com)

0148-0227/12/2011JC007751

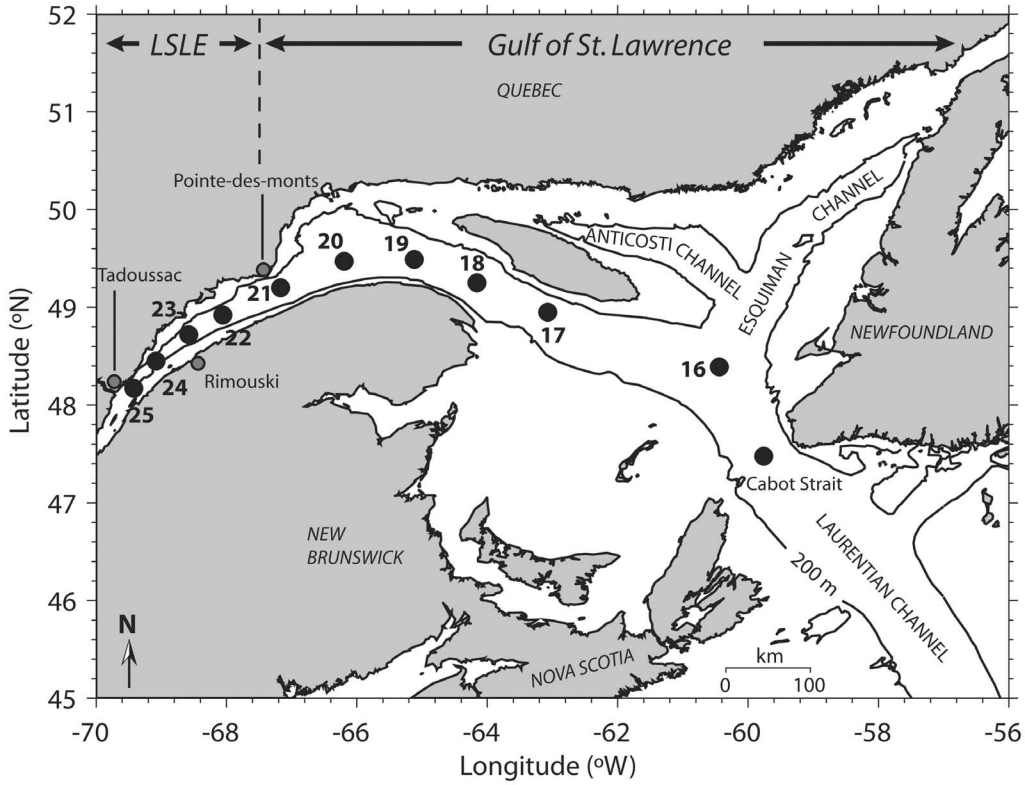

Figure 1. Map of the Lower Estuary and Gulf of St. Lawrence in Eastern Canada, showing the sampled stations along the Laurentian Channel.

can only be replenished by diffusion from the oxygenated surface layer and by landward advection from the oxygenated Atlantic waters [*Bugden*, 1991].

[4] The transport of a tracer in the bottom waters of the Laurentian Channel can be described by a simple advection-diffusion equation [*Bugden*, 1991]. Thus, variations of the bottom water dissolved oxygen concentration along the Laurentian Channel can be modeled as a laterally averaged 2-D fluid influenced by horizontal and vertical diffusion as well as horizontal advection [*Benoit et al.*, 2006] (see Figure 2 for a description of their model). With this simple model, *Benoit et al.* [2006] successfully generated hypoxia in the LSLE but could not reproduce the tongue of oxygen minimum water that is observed between 250 and 275 m depth or along the $\sigma_t \approx 27.25$ kg m^{-3} isopycnal (Figure 3). They made two major simplifications which could explain the lack of fine-scale vertical structure in their model simulations: (1) they applied a constant advection velocity (the bathymetry was flat and the vertical advection was null) and (2) assumed that the only significant oxygen sink was the sediment (benthic respiration), i.e., they neglected pelagic (water column) respiration (Figure 2). In a recent study, *Lehmann et al.* [2009] reported that pelagic respiration may account for up to 40% of the oxygen consumption in the deep waters of the Laurentian Channel. Hence, to reproduce the distribution of dissolved oxygen concentrations throughout the LSLE as well as identify and determine the relative contributions of the processes responsible for the generation of this mid-water column oxygen minimum, we developed a simple 2-D numerical model that includes both pelagic and benthic oxygen respiration and in which we implemented a more realistic bathymetry of the Laurentian Channel.

2. Model Description

[5] Our numerical model is a 2-D representation of oxygen transport in the bottom waters of the Laurentian Channel, where the advection and diffusion of dissolved oxygen, respectively from the Atlantic Ocean and the surface waters, are counterbalanced by benthic and pelagic respiration (Figure 4). The bottom waters flow landward from Cabot Strait and upwell at the head of the Laurentian Channel (Figure 1). Cabot Strait and Station 25, respectively, correspond to the eastern and western boundaries of the model, where the bottom waters extend from the permanent pycnocline at 150 m to the seafloor. Station 25 was set as the western boundary because of its location before the abrupt change in bathymetry, allowing us to neglect the influence of upwelling in the water circulation landward of this station.

2.1. Oxygen Transport

[6] As proposed by *Bugden* [1991] and applied by *Benoit et al.* [2006], the transport of oxygen in the bottom waters of the Laurentian Channel was represented by a 2-D advection-diffusion equation:

$$\frac{\partial O_2}{\partial t} = -\vec{\nabla}.(\vec{u}O_2) + K\ \nabla^2 O_2 + SMS(O_2) \qquad (1)$$

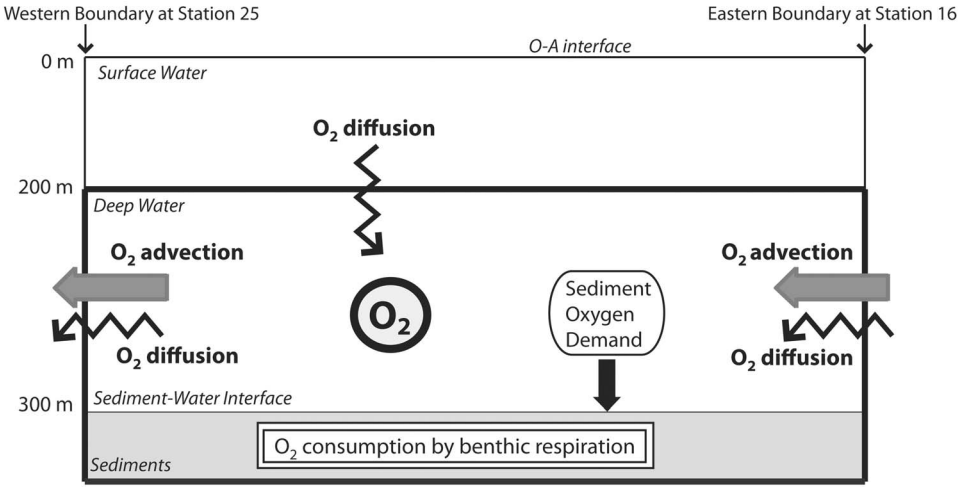

Figure 2. Schematic diagram of the advection-diffusion numerical model solved by *Benoit et al.* [2006]. The bold line represents the model boundaries. The gray area represents the benthic (sediment) oxygen sink. The strength of the sediment oxygen sink was calculated from a diagenetic model (see Figure 5 for the value of the benthic sink and *Benoit et al.* [2006] for a detailed model description).

where K is a diagonal matrix of eddy diffusivity coefficients, $\vec{u}$ is the velocity vector and SMS is the source minus sink term due to the biogeochemical processes. The solution to equation (1) is simplified by making the following assumptions about the flow:

[7] 1. The system is assumed stationary since the properties of the bottom waters vary mainly on decadal to secular time scales [*Benoit et al.*, 2006; *Gilbert et al.*, 2005; *Koutitonsky and Bugden*, 1991].

[8] 2. The deep waters of the Laurentian Channel are considered as a laterally averaged 2-D uniform fluid [*Bugden*, 1991], with a vanishing cross-channel velocity. We also assume that the funnel effect (slowly changing depth) will only affect the vertical and along-channel velocity components.

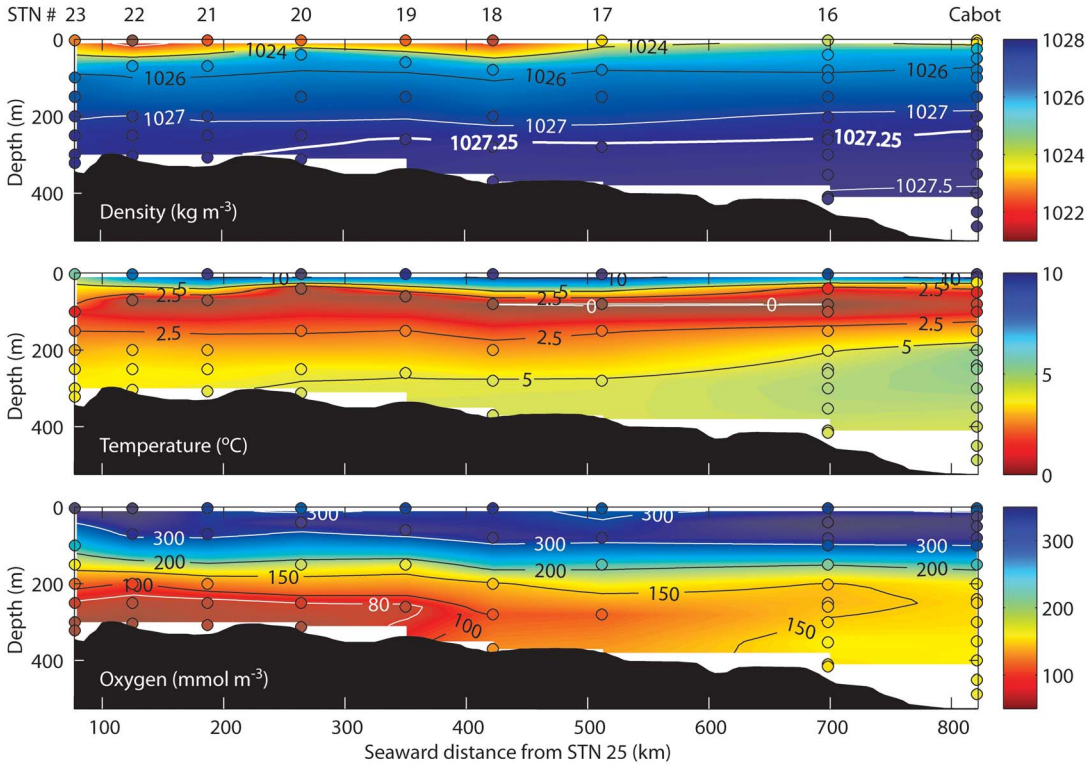

Figure 3. Density, temperature and oxygen concentrations measured along the Laurentian Channel (from Station 23 to Cabot Strait) in July 2010.

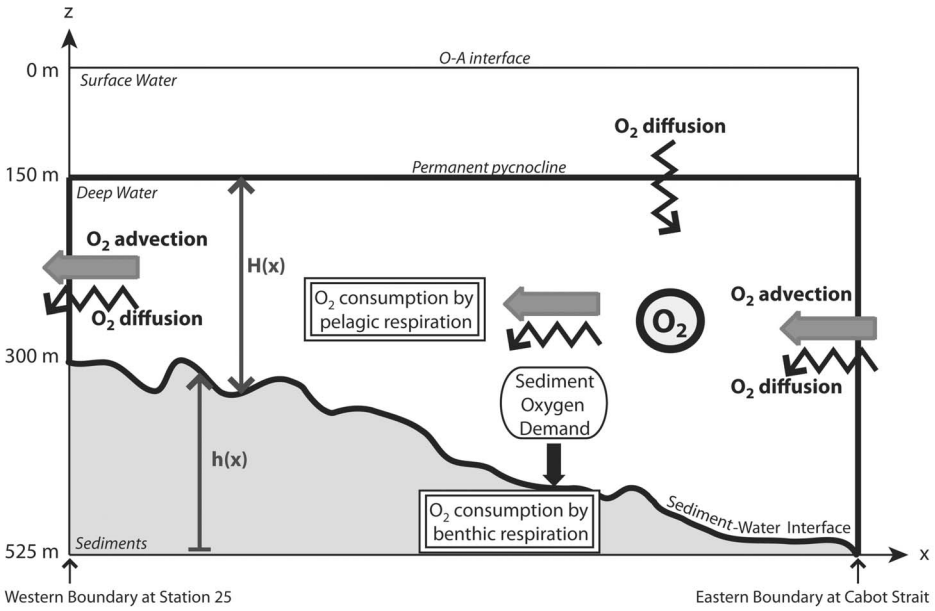

Figure 4. Schematic diagram of the advection-diffusion numerical model used in this study. The bold line represents the model boundaries. The gray area represents the benthic (sediment) oxygen sink. The variables h(x) and H(x) are defined in Table 3.

[9] 3. The upper boundary of the model (at 150 m) is considered rigid so that the advection velocity depends on the transport at Cabot Strait, the water column height, and the width of the channel. The horizontal velocity was calculated from the transport with a variable depth and constant width (Table 1, equation (3)). The Laurentian Channel width was assumed constant with depth: the V-channel is approximated as a U-channel [*Bugden*, 1991]. The width of the Laurentian Channel was also assumed constant between Cabot Strait and Station 25 since it is nearly constant over four fifths of its length (from Cabot Strait to the mouth of the LSLE). The bathymetry follows the maximum depth along the central axis of the Laurentian Channel from Station 25 (300 m) to Cabot Strait (525 m) at a 1-km spatial resolution. The bottom topography data were provided by the Canadian Hydrographic Service of Fisheries and Oceans Canada. The vertical velocity was computed from the continuity equation (Table 1, equation (4)) and satisfies the boundary conditions at the pycnocline and the sediment-water interface (Table 1, equations (7) and (9)), so that the component of the total velocity (u, w) perpendicular to the boundary is zero at the bottom [*LeBlond and Mysak*, 1978].

[10] 4. The horizontal diffusion coefficient K_x is enhanced to reflect the impact of the cross-channel flow [*Benoit et al.*, 2006; *Bugden*, 1991]. This coefficient is assumed constant in the bottom waters and is calculated from the mean advection velocity and the channel width, as proposed by *Bugden* [1991] (Table 1, equations (5) and (6)).

[11] Under these assumptions, equation (1) simplifies to:

$$u(x)\frac{\partial[O_2]}{\partial x} + w(x,z)\frac{\partial[O_2]}{\partial z} = K_x\frac{\partial^2[O_2]}{\partial x^2} + K_z\frac{\partial^2[O_2]}{\partial z^2} + R_{wc} \quad (2)$$

Table 1. Model Equations, Boundary Conditions and Initial Conditions[a]

Equation	Notes
Transport	
Advection	
$u(x) = \frac{F_0}{H(x)\times W}$ (3)	W is the channel width
$w(x,z) = -(H_{\max} - z)\frac{\partial u(x)}{\partial x}$ (4)	deduced from $\frac{\partial u}{\partial x} + \frac{\partial w}{\partial z} = 0$
Diffusion	
$K_x = \frac{\overline{u}^2 W^2}{120\ K_l}$ (5)	$\overline{u}$ is the mean advection velocity along the Laurentian Channel and K_l is the lateral diffusion coefficient [see *Bugden*, 1991]. Substituting equation (3) into equation (5), we obtain equation (6)
$K_x = \frac{\left(F_0/\overline{H}\right)^2}{120\ K_l}$ (6)	$\overline{H}$ is the averaged deep water column height along the Laurentian Channel
Boundary Conditions	
At z = 150 m	
$w = 0$ (7)	
$[O_2]_{150\ m} = 170$ mmol O_2 m^{-3} (8)	
At the sediment-water interface $z = h(x)$	
$w(x) = u(x)\frac{\partial h(x)}{\partial x}$ (9)	
$R_{sed} = -3540$ mmol O_2 m^{-2} yr^{-1} (10)	
At Station 25 (x = 0 km)	
$u(0) = \frac{F_0}{H(0)\times W}$ (11)	
At Cabot Strait ($x = L$ = 825 km)	
$u(L) = \frac{F_0}{H(L)\times W}$ (12)	
$[O_2]_L = 170$ mmol O_2 m^{-3} (13)	
Initial Conditions	
$[O_2]_{init} = 170$ mmol O_2 m^{-3} (14)	assumed to be the same over the entire domain

[a]Here, x stands for the seaward distance from Station 25 along the central axis of the Laurentian Channel and z stands for the depth, upward. See Tables 2 and 3 for undefined parameters and variables.

Table 2. List of Parameters With Definitions, Values, Units and Literature Sources

Parameter	Definition	Value	Unit	Reference
	Physics			
F_0	Transport below the 150 m depth at Cabot Strait	$0.11 \cdot 10^6$	$m^3\ s^{-1}$	*Bugden* [1991]
$\overline{u}$	Averaged horizontal velocity along the Laurentian Channel	$0.53 \cdot 10^{-2}$	$m\ s^{-1}$	*Bugden* [1991]
K_x	Horizontal diffusion coefficient	$16 \cdot 10^2$	$m^2\ s^{-1}$	*Bugden* [1991]
K_z	Vertical diffusion coefficient	$1.0 \cdot 10^{-4}$	$m^2\ s^{-1}$	*Bugden* [1991]
W	Width of the Laurentian Channel	$97.5 \cdot 10^3$	m	Figure 1; see section 2.1
	Biogeochemistry			
R_{WC}	Respiration in the water column, i.e., pelagic respiration	−19.6	mmol $O_2\ m^{-3}\ yr^{-1}$	*Lehmann et al.* [2009]
R_{sed}	Sediment oxygen demand, i.e., benthic respiration	−3540	mmol $O_2\ m^{-2}\ yr^{-1}$	*Lehmann et al.* [2009]

[12] Note that the *SMS* term from equation (1) was replaced by R_{wc}, which corresponds to the sink induced by pelagic respiration; the benthic sink does not appear in the transport equation since it is included in the model as a boundary condition at the sediment-water interface (see Table 1, equation (10) and sections 2.2.2 and 2.3). K_z represents the constant vertical diffusion coefficient (Table 2). The variables (x, u) and (z, w) are used for the horizontal and vertical positions and velocity components, respectively. For other parameter and variable descriptions, see Tables 1, 2 and 3.

2.2. Oxygen Sinks

2.2.1. Pelagic Respiration

[13] Based on modeling of the dissolved oxygen isotope compositions, *Lehmann et al.* [2009] calculated that 1960 mmol $O_2\ m^{-2}\ yr^{-1}$ are consumed in the 100 m water layer above the sediment-water interface between Stations 23 and 16 (Figure 1). The respiration rate was assumed equally distributed in this water layer (19.6 mmol $m^{-3}\ yr^{-1}$) and the latter value was assigned to the pelagic sink value R_{wc} (equation (2)) over the entire model domain. R_{wc} is assumed to be invariant with depth (z) and distance (x), as implemented in previous studies [*Savenkoff et al.*, 1995, 1996]. The latter authors showed that the pelagic respiration rate is constant with depth from 150 m to the sediment-water interface throughout the Lower Estuary and the Gulf of St. Lawrence. Based on ETS (electron transport system) measurements, they estimated that about 40 mmol $O_2\ m^{-3}\ yr^{-1}$ are consumed in the Lower Estuary whereas between 35 and 55 mmol $O_2\ m^{-3}\ yr^{-1}$ are consumed in the Gulf at depths below 150 m. ETS measurements are known to overestimate respiration in marine water [*Packard*, 1985; *Vosjan and Nieuwland*, 1987; *Vosjan et al.*, 1990], but *Packard* [1985] empirically demonstrated that the R:ETS (respiration to ETS) ratio is equal to 0.75 for bacteria. Accordingly, we applied this ratio to correct the measurements of *Savenkoff et al.* [1995, 1996] and derived an averaged respiration rate of 32.5 ± 7.8 mmol $O_2\ m^{-3}\ yr^{-1}$, within a factor of two of the rate (19.6 ± 5.6 mmol $O_2\ m^{-3}\ yr^{-1}$) derived by *Lehmann et al.* [2009].

2.2.2. Benthic Respiration

[14] Benthic oxygen fluxes measured along the Laurentian Channel [*Anschutz et al.*, 2000; *Katsev et al.*, 2007; *Silverberg et al.*, 2000] display as much spatial variations at the small-scale (1 m; within the sampling diameter of a multicorer) than at larger spatial scales (50–100 km; i.e., between stations) and show no clear trend from Station 25 to Cabot Strait (Figure 5; for details see G. Chaillou et al., Fluxes and distributions of dissolved oxygen, nitrate, phosphate, iron, and manganese in Laurentian Trough sediments exposed to different bottom water oxygen concentrations, submitted to *Aquatic Geochemistry*, 2011), despite documented variations in the nature (terrestrial:marine) and accumulation rates of organic matter along the Laurentian Channel [*Colombo et al.*, 1996a, 1996b; *Lucotte et al.*, 1991; *Muzuka and Hillaire-Marcel*, 1999; *Silverberg et al.*, 2000; *Smith and Schafer*, 1999] (see Table 3 in *Benoit et al.* [2006] for a compilation of organic carbon accumulation rates). Hence, we assumed that the oxygen uptake rate from the sediment is constant along the Laurentian Channel (Table 1, equation (10)).

[15] The spatially averaged oxygen flux derived from sediment core incubations (1374 ± 624 mmol $O_2\ m^{-2}\ yr^{-1}$) is 2.5 times smaller than the benthic respiration estimated by *Lehmann et al.* [2009] (3540 ± 560 mmol $O_2\ m^{-2}\ yr^{-1}$). We believe that benthic oxygen fluxes measured from sediment core incubations might underestimate the sediment oxygen demand because of sampling artifacts. *Glud et al.* [1994] showed that total oxygen uptake rates measured in the laboratory were lower than those measured in situ because of underrepresentation and disturbance of the macrofauna. Variability of macrofauna density in incubation experiments, carried out on multiple sediment cores recovered from the same station, might also explain the high intrasite variability in oxygen uptake rates (Chaillou et al., submitted manuscript, 2011). Consequently, we chose the benthic respiration rate estimated by *Lehmann et al.* [2009] as a boundary condition for the benthic oxygen flux. Hence, both the pelagic and benthic respiration rates used in our model were estimated by the same method (i.e., modeling of the dissolved oxygen isotope compositions).

Table 3. List of State Variables With Definitions and Units[a]

Variable	Definition	Unit
$[O_2]$	Dissolved oxygen concentration	mmol $O_2\ m^{-3}$
$[O_2]_{init}$	Initial dissolved oxygen concentration	mmol $O_2\ m^{-3}$
$u(x)$	Horizontal velocity along the Laurentian Channel	$m\ s^{-1}$
$w(x)$	Vertical velocity along the Laurentian Channel	$m\ s^{-1}$
$H(x)$	Deep water column height	m
$h(x)$	Superficial sediment height above the maximal depth	m

[a]Here, x represents the seaward distance from Station 25 along the Laurentian Channel.

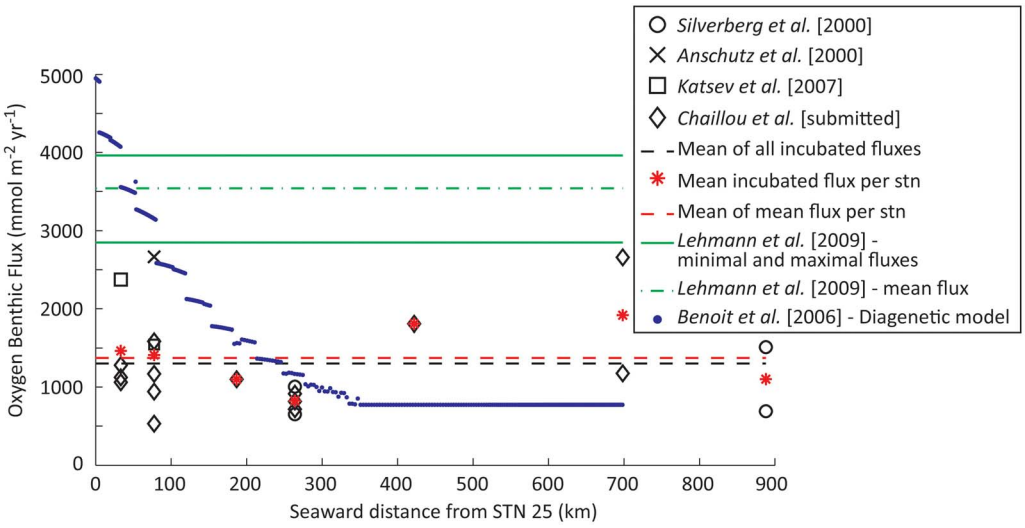

Figure 5. Dissolved oxygen flux at the sediment-water interface measured from sediment core incubations (black symbols); derived from the dissolved oxygen isotopic composition (green lines) and calculated from the carbon rain rate with a simplified diagenetic model (blue dots).

2.3. Initial and Boundary Conditions

[16] The vertical oxygen concentration at Cabot Strait is nearly invariant with depth below 150 m (169 ± 18 mmol O_2 m^{-3}), and, with the exception of a few small scale variations, the oxygen concentration at 150 m depth between Station 25 and Cabot Strait does not vary significantly (168 ± 34 mmol O_2 m^{-3}; Figure 6; D. Gilbert and E. Nault, Oxygen Atlas for the Gulf of St. Lawrence, unpublished data, 2007). Consequently, the oxygen concentration at these boundaries was set at 170 mmol m^{-3} (Table 1, equations (8) and (13)). Since the system is stationary, these boundary conditions were applied as initial conditions within the model domain for all variables (Table 1, equation (14)). At the head of the Estuary (Station 25), the boundary is open as the numerical grid ends but fluid motion remains unrestricted [*Chapman*, 1985]. We impose a no-gradient Neumann condition: $\frac{\partial [O_2]_{x=0}}{\partial x} = 0$. Dirichlet conditions were imposed at the three other boundaries (at Cabot Strait, along the pycnocline and at the sediment-water interface).

2.4. Tuning of Physical Parameters

[17] In order to tune the physical model parameters, simulation runs were performed with physical parameters (F_0, $\overline{u}$, W, K_x, K_z) whose assigned values covered the range reported in the literature (Table 4). The outputs of these simulations were compared statistically to a reference state chosen to be the 2002–2010 oxygen climatology (Figure 6). The climatology was preferred to a specific-year transect to neglect small seasonal and inter-annual variabilities since temporal variations are not represented in our steady state model. The similarity between the model output and the climatology is quantified in terms of the mean (M), the bias ($M_{model} - M_{data}$), the root mean square (RMS) difference, the centered pattern RMS difference ($E' = \sqrt{(RMS^2 - bias^2)}$), the standard deviation (σ) and the correlation (R). The statistical information (σ, R, E') is summarized on a Taylor diagram [*Taylor*, 2001], which graphically summarizes how closely a pattern (or a set of patterns) matches observations (Figure 7). Using the benthic and pelagic respiration rates estimated by *Lehmann et al.* [2009], the model best fit (simulated dissolved oxygen concentrations) to the observations (identified as model-ref in Figure 7) is given for the parameter values listed in Table 2. The chosen model-ref presents the best combination of high correlation (R = 0.899), low bias (2.07 mmol O_2 m^{-3}), small centered RMS difference (E' = 0.438) and low standard deviation (σ = −3.10 mmol O_2 m^{-3}).

[18] If the spatially averaged benthic oxygen uptake rate derived from sediment core incubation experiments is substituted for the value derived by *Lehmann et al.* [2009], the best fit to the data is given for a transport F_0 = 0.035 Sv (1 Sv = 10^6 m^3 s^{-1}), corresponding to an averaged along-channel advection velocity of 0.17 cm s^{-1} (not shown). This advection velocity is much smaller than the values computed by *Bugden* [1991] (0.5 cm s^{-1}) and *Gilbert* [2004] (1.0 cm s^{-1}) from the temperature field, further supporting the hypothesis that oxygen fluxes derived from sediment core incubations might be underestimated.

2.5. Model Implementation

[19] The model was implemented within the Matlab® programming environment using the finite element code for elliptic equations from their Partial Differential Equations Toolbox [*MathWorks, Inc.*, 2006]. The toolbox has also a function for global, uniform mesh refinement. The refinement ends when each triangle contributes less than 10^{-3}, the preset tolerance. More details on the finite element method may be found in *Johnson* [1987].

3. Model-Data Comparison

[20] Our model properly reproduces the spatial distribution of dissolved oxygen in the bottom waters of the Laurentian Channel (Figures 6 and 8). The simulated oxygen concentration decreases as the bottom waters travel landward and reaches the hypoxic threshold in the LSLE. The vertical modeled-profiles of oxygen reproduce the observed

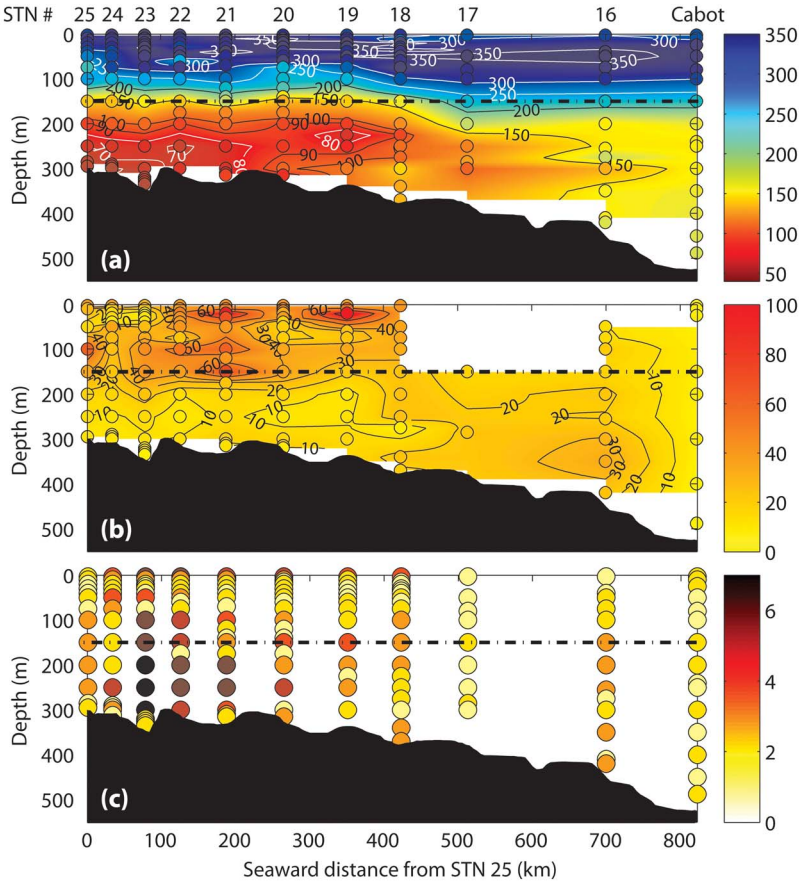

Figure 6. Dissolved oxygen climatology from 2002 to 2010 in the bottom waters of the Laurentian Channel: (a) mean oxygen concentration in mmol O_2 m^{-3}, (b) standard deviation in mmol O_2 m^{-3} and (c) number of measurements. The dashed lines follow the 150 m depth. Dissolved oxygen concentrations were determined by Winkler titrations [*Grasshoff et al.*, 1999].

oxygen minimum between 250 and 275 m depth (Figure 8). In agreement with the climatology (Figure 6), the oxygen minimum depth increases with the water column thickness (Figure 8). Nevertheless, from Station 17 to Cabot Strait, the simulated oxygen concentration is underestimated in the first tens of meters below the pycnocline. This small discrepancy is caused by our choice of boundary conditions, i.e., setting the dissolved oxygen concentration at a fixed value of 170 mmol O_2 m^{-3} along the pycnocline while, in reality, it is ~215 mmol O_2 m^{-3} between Station 17 and Cabot Strait (Figure 6). Despite the simplified representation of the deep water circulation, the compatibility of the modeled and observed oxygen concentrations confirms that dissolved oxygen is only provided to the bottom waters of the Laurentian Channel through advective and diffusive processes, as proposed by *Bugden* [1991].

4. Sensitivity Analysis

[21] We performed a sensitivity analysis to assess the impact of physical (advection and diffusion) and biogeochemical processes (benthic and pelagic respiration) on the distribution of dissolved oxygen in the deep waters of the Laurentian Channel. Physical and biogeochemical parameters of the model were modified individually over the range of values reported in the literature (Tables 4, 5 and 6). The simulated dissolved oxygen concentrations from each run are compared with the reference run, referred to as

Table 4. Range of Physical Parameter Values Tested in Model Tuning

Parameter	Range of Values Tested	Unit	Reference
F_0	0.11–0.22	10^6 m^3 s^{-1}	*Bugden* [1991], *Gilbert* [2004], *Han et al.* [1999], *Saucier et al.* [2003]
$\overline{u}$	0.47–2.06	10^{-2} m s^{-1}	*Bugden* [1991], *Gilbert* [2004], *Han et al.* [1999], *Saucier et al.* [2003]
K_x	4.27–81	10^2 m^2 s^{-1}	*Bugden* [1991]
K_z	0.45–2.2	10^{-4} m^2 s^{-1}	*Bugden* [1991], *Savenkoff et al.* [2001]
W	50–110	10^3 m	Figure 1

Table 5. Range of Parameter Values Used for the Sensitivity Analysis of Physical Parameters[a]

Parameter	Variation (%)	Parameter Value	$\overline{u}$ (cm s^{-1})	u_{min} (cm s^{-1})	u_{max} (cm s^{-1})	K_x (10^2 m^2 s^{-1})
F_0 (*Sv* or 10^6 m^3 s^{-1})	ref	0.11	0.53	0.30	0.76	16 ∼ ref
for W = 97.5 km	+10	0.12	0.58	0.33	0.84	19 ∼ + 20%
	+20	0.13	0.63	0.36	0.91	23 ∼ + 45%
	+50	0.17	0.79	0.45	1.14	36 ∼ + 125%
	+100	0.22	1.05	0.60	1.52	64 ∼ + 300%
W (km) for F_0 = 0.11 Sv	−50	48.8	1.05	0.60	1.52	16
	−20	78	0.66	0.38	0.95	16
	−10	87.8	0.59	0.33	0.85	16
	ref	97.5	0.53	0.30	0.76	16
	+5	103	0.50	0.28	0.72	16
K_z (cm^2 s^{-1})	−90	0.1	-	-	-	-
	−55	0.45	-	-	-	-
	ref	1	-	-	-	-
	+120	2.2	-	-	-	-
	+400	5	-	-	-	-

[a]Here, ref stands for reference: F_0 = 0.11 Sv (Sverdrup: 10^6 m^3 s^{-1}), W = 97.5 km and K_z = 1 cm^2 s^{-1}; $\overline{u}$, $u_{min}$and u_{max} are, respectively, the spatially averaged, the minimum and the maximum advection velocities. Refer to Table 2 for other parameters values.

model-ref (Figure 8). Sensitivity analysis results are presented on Taylor diagrams (Figure 9) [*Taylor*, 2001].

4.1. Physical Parameters

[22] Tested physical parameters included the transport (F_0), the coefficient of vertical diffusion (K_z) and the channel width (W), since a modification of any of these values can potentially change the oxygen transport mode. Indeed, the along-channel advection rate of oxygen varies with the water advection velocity, which changes if either F_0 or W is modified (Table 1, equations (3) and (4)). The horizontal diffusion rate of dissolved oxygen varies with the horizontal diffusion coefficient (K_x), which changes with F_0 (Table 1, equation (6)). Finally, the vertical diffusion of dissolved oxygen varies with K_z. The vertical diffusion coefficient was varied between 0.1 cm^2 s^{-1}, a typical value for the deep ocean [*Ledwell et al.*, 1993], and 5 cm^2 s^{-1}, a value that reflects intense vertical mixing [*Large et al.*, 1994]. The reference transport value was varied from 0% to 100% to include the range of horizontal advection velocities estimated by *Bugden* [1991] and *Gilbert* [2004], respectively. The channel width was varied from 50 km to ∼105 km to encompass the true range from the Lower Estuary to Cabot Strait. Refer to Table 5 for the range of parameter values.

Table 6. Range of Parameter Values Used for the Sensitivity Analysis of Biological Parameters[a]

Tested Respiration (R_{wc}, R_{sed})	Pelagic Respiration (mmol O_2 m^{-3})	Benthic Respiration (mmol O_2 m^{-2} yr^{-1})	Total Respiration (mmol O_2 m^{-2} yr^{-1})	R_{sed}:R_{wc}
		Lehmann et al. [2009]		
ref	**19.6**	**3450**	**5410**	**1.8**
(−21%, ref)	15.4	3450	4990	2.2
(+35%, ref)	26.5	3450	6100	1.3
(ref, +12%)	19.6	3960	5920	2.0
(ref, −20%)	19.6	2850	4810	1.5
(−21%, +12%)	15.4	3960	5500	2.6
(+35%, −20%)	26.5	2850	5500	1.1
(−21%, −20%)	15.4	2850	4390	1.9
(+35%, +12%)	26.5	3960	6610	1.5
		ETS + Incubations		
(+26%, −80%)	24.7	750	3220	0.3
(+105%, −44%)	40.3	1998	6028	0.5
(+105%, −80%)	40.3	750	4780	0.2
(+26%, −44%)	24.7	1998	4468	0.8
		Lehmann et al. [2009] + *Benoit et al.* [2006]		
(−20%, F_{O2} = f(x))	15.4	772–4946	5905	2.8
(ref, F_{O2} = f(x))	19.6	772–4946	6325	2.2
(+12%, F_{O2} = f(x))	26.5	772–4946	7015	1.6
		Benthic or Pelagic Respiration Alone		
(ref, −100%)	19.6	0	1960	0
(−100%, ref)	0	3540	3540	-
(−100%, F_{O2} = f(x))	0	772–4946	4365	-

[a]Here, ref stands for reference; reference values are in bold. F_{O2} = f(x) stands for an along-channel variable benthic respiration and is defined from the diagenetic model of *Benoit et al.* [2006] (the function is plotted on Figure 5).

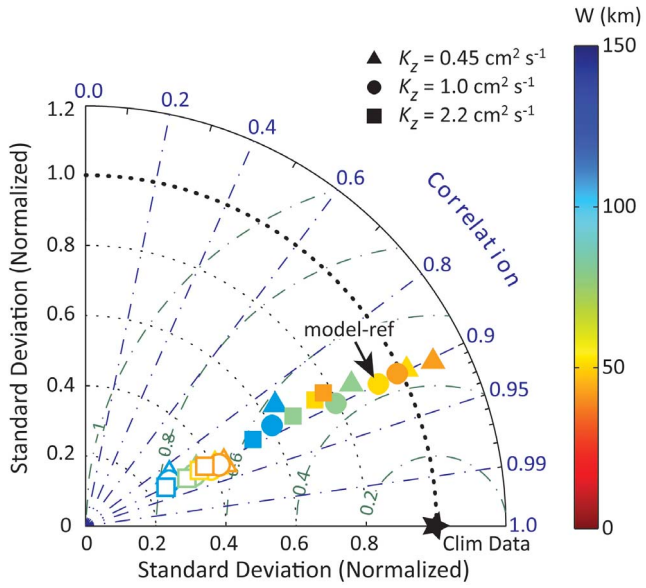

Figure 7. Taylor's diagram for dissolved oxygen concentrations, showing the tuning of physical parameters. Filled symbols are for F_0 = 0.11 Sv and open symbols for F_0 = 0.22 Sv. Pelagic and benthic respiration rates are fixed to the mean values given by *Lehmann et al.* [2009]: R_{wc} = −19.6 mmol O_2 m^{-3} yr^{-1} and R_{sed} = −3540 mmol O_2 m^{-2} yr^{-1}. The radial distance from the origin is proportional to the standard deviation (σ) of a pattern (normalized by the standard deviation of the climatology). The bold dotted line represents σ = 1. The green lines are the distances from the reference point and indicate the centered pattern RMS difference E′ (i.e., the RMS error once overall bias has been removed; see the mathematical expression in section 2.4 for more details). The correlation between the climatology data and the model output is given by the azimuthal position of the model output. The model output giving the best fit to the data is labeled model-ref. For this simulation, the bias (M_{model} - M_{data}) is 2.07 mmol O_2 m^{-3}.

[23] An increase of the horizontal diffusion coefficient (represented on Figure 9a by the distance between the yellow and green symbols at a same advection velocity, i.e., compare yellow triangle with green square and yellow diamond with green triangle) enhances the oxygenation of the bottom waters but has the smallest impact of the three tested physical parameters (i.e., advection velocity, horizontal and vertical diffusion coefficients) on the oxygen distribution. As variations in the transport (Figure 9a, green symbols) embrace variations of the advection velocity and the horizontal diffusion coefficient, they have a greater influence on the oxygen distribution than variations of the advection velocity (yellow symbols) or horizontal diffusion alone. The linear variation of the three statistic metrics (σ, R, E'), combined to high correlation coefficients (>0.977) and high bias (Figure 9a, green symbols) between model simulations and model reference, reveal that variations in the transport slightly modify the shape of the oxygen profile (i.e., vertical distribution) but greatly impact the oxygen concentrations throughout the Channel (i.e., horizontal distribution): the higher the transport, the higher the advection velocity, the higher the dissolved oxygen renewal rate and concentrations. In contrast, variations of the vertical diffusion coefficient (Figure 9a, black symbols) modify both the shape of the profiles (high variations of the three statistic metrics (σ, R, E')) and the dissolved oxygen concentrations (high variations of the bias). Hence, the vertical diffusion seems to be the physical parameter that influences most the dissolved oxygen distribution. Results of our sensitivity analysis agree with those of *Benoit et al.* [2006] who showed that, in the LSLE, the dissolved oxygen concentration is very sensitive to vertical mixing when the vertical eddy diffusivity, K_z, is smaller than 3 cm^2 s^{-1}. Consequently, the vertical diffusion coefficient, K_z, needs to be better constrained. For reasonable variations of the physical parameter values (i.e., −55 to 120% for vertical diffusivity, 0 to 20% for the transport and −20 to +5% for the channel width), the discrepancies between the spatially averaged modeled and observed oxygen concentrations are less than 15%.

4.2. Biogeochemical Parameters

[24] Benthic and pelagic respiration rates were varied in order to estimate their impact on the dissolved oxygen distribution. This is equivalent to modifying the location and strength of the oxygen sinks. In our simulations, the pelagic and benthic respiration rates were varied either independently or simultaneously. The benthic respiration rate was varied between 750 and 3960 mmol O_2 m^{-2} yr^{-1} (i.e., −80 to +12% from the reference), whereas the pelagic respiration rate was varied between 15.4 and 40.3 mmol O_2 m^{-3} yr^{-1} (i.e., −21% and +105% from the reference). The chosen ranges cover realistic variations estimated by *Lehmann et al.* [2009] (green symbols on Figure 9b), the range of estimated benthic and pelagic respiration measurements (open black symbol on Figure 9b), as well as the influence of a spatially variable benthic respiration (filled yellow symbols on Figure 9b; the function F_{O2} = f(x) is plotted on Figure 5 (blue dots) and has a spatially averaged value of 4365 mmol O_2 m^{-2} yr^{-1}). The range of respiration rates estimated from direct measurements (incubations and ETS) is shown to give the best possible representation of the impact of biogeochemistry on the oxygen distribution even though it yields improbable, much smaller benthic:pelagic respiration rate ratios (<1) than the value (1.5) estimated by *Lehmann et al.* [2009]. The simulations with either benthic or pelagic respiration alone are presented for information (filled black symbols on Figure 9b). Refer to Table 6 for the range of respiration values.

[25] Within the range investigated, the respiration rates have little impact on the spatial dissolved oxygen distribution pattern, but mostly affect the absolute oxygen concentrations. With the more realistic bathymetry, the oxygen minimum is always generated regardless of the location or the strength of the oxygen sink (excepted when both benthic and pelagic sinks are null), and its location within the water column varies at most by 15 m. The greatest variation in the depth of the oxygen minimum occurs when either benthic or pelagic respiration are null (respectively filled black triangle and filled black circle and diamond on Figure 9b), and although such a situation is unrealistic, the correlation coefficient between the simulated and reference oxygen

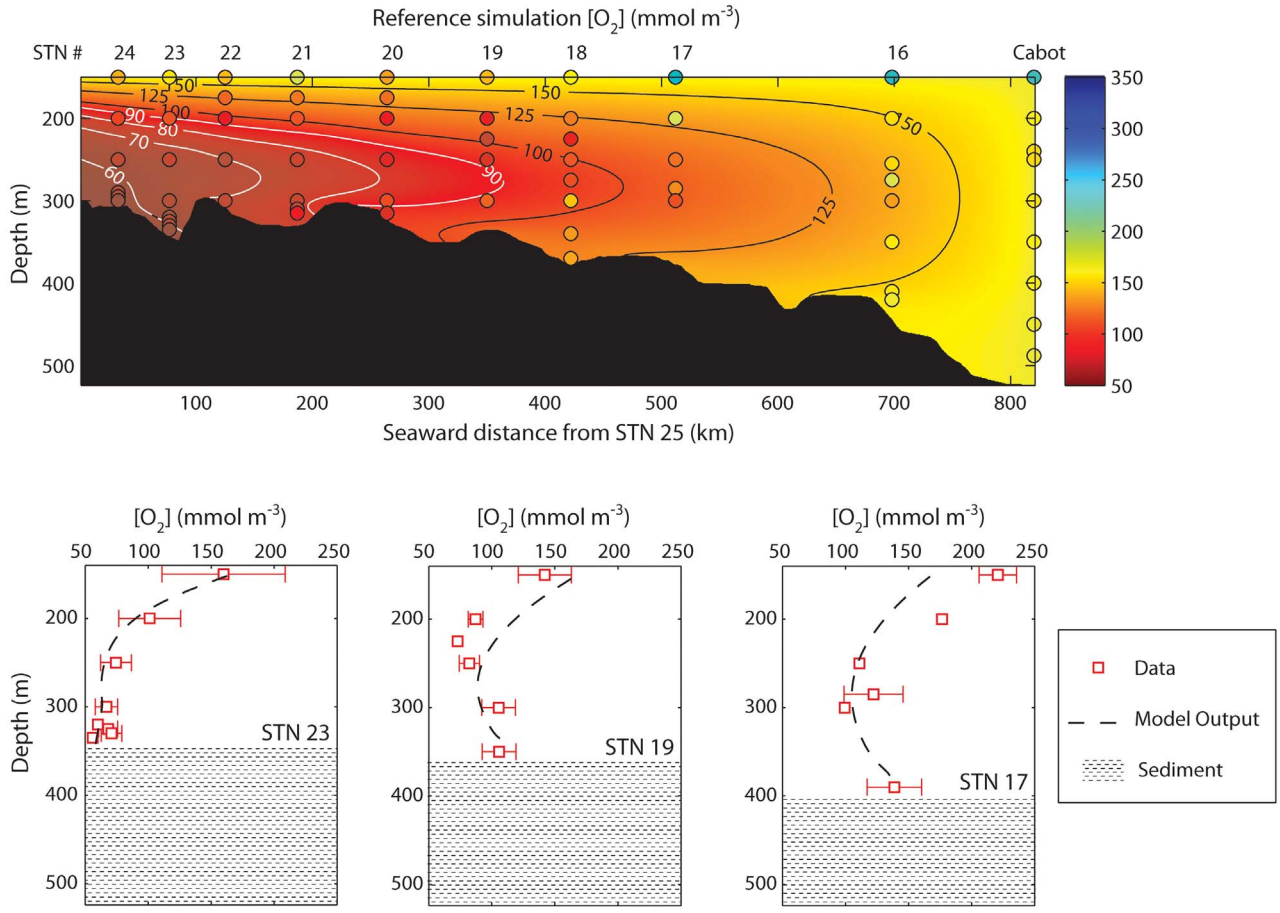

Figure 8. Dissolved oxygen distribution for the reference simulation with the following parameters: F_0 = 0.11 Sv, W = 97.5 km and K_z = 1 cm^2 s^{-1}, R_{wc} = −19.6 mmol O_2 m^{-3} yr^{-1} and R_{sed} = −3540 mmol O_2 m^{-2} yr^{-1} (see Tables 2 and 3 for definitions). (top) Colored circles for the climatology are overlaid on the simulated dissolved oxygen field using the same color scale. (bottom) Comparison of simulated dissolved oxygen vertical profiles with observations at Stations 23, 19 and 17.

distribution patterns remains above 0.956. Variations of the benthic:pelagic respiration rate ratio (filled green symbols, open black symbols and yellow symbols on Figure 9b), from the reference value of 3:2 estimated by *Lehmann et al.* [2009], induce small changes in the spatial distribution of oxygen, as reflected by the high correlation coefficient (>0.974). The largest deviations from the modeled reference values are observed when the total respiration rate (i.e., spatially integrated pelagic + benthic rates) is either minimal (3220 mmol O_2 m^{-2} yr^{-1}, open black triangle on Figure 9b) or maximal (7015 mmol O_2 m^{-2} yr^{-1}, filled yellow diamond on Figure 9b). The minimal total respiration rate is smaller than the estimated benthic respiration rate (3540 mmol O_2 m^{-2} yr^{-1}, filled black circle on Figure 9b) and, thus, too low to be considered as a plausible situation. Variations of the benthic respiration rate along the channel do not significantly affect the distribution and concentration of dissolved oxygen in the bottom waters (filled yellow symbols on Figure 9b). The modeled dissolved oxygen concentrations mostly depend on the strength of the total oxygen sink, and for reasonable values of the oxygen sinks (i.e., between 4390 and 7015 mmol O_2 m^{-2} yr^{-1}), the discrepancy between the spatially averaged modeled and observed oxygen concentrations is less than 11%.

5. Interpretation and Implication of the Oxygen Minimum

[26] In order to explain the generation of a mid-water column oxygen minimum, we examined the mechanisms governing the spatial distribution of dissolved oxygen in the deep waters of the Laurentian Channel by establishing an oxygen mass budget in two sub-domains divided by the 275 m depth (Figure 10), corresponding approximately to the oxygen minimum (Figure 8). The budget allows us to identify which process drives the oxygen supply, sink and transport, and thus improves our understanding of the role of each physical process on the spatial distribution of dissolved oxygen. We focus on the role of physical processes in the bottom waters of the Laurentian Channel because results of our sensitivity analysis (see section 4) show that the dissolved oxygen concentrations and distribution pattern are much more sensitive to variations of physical than biogeochemical parameters, and that the latter only slightly modify the position of the oxygen minimum.

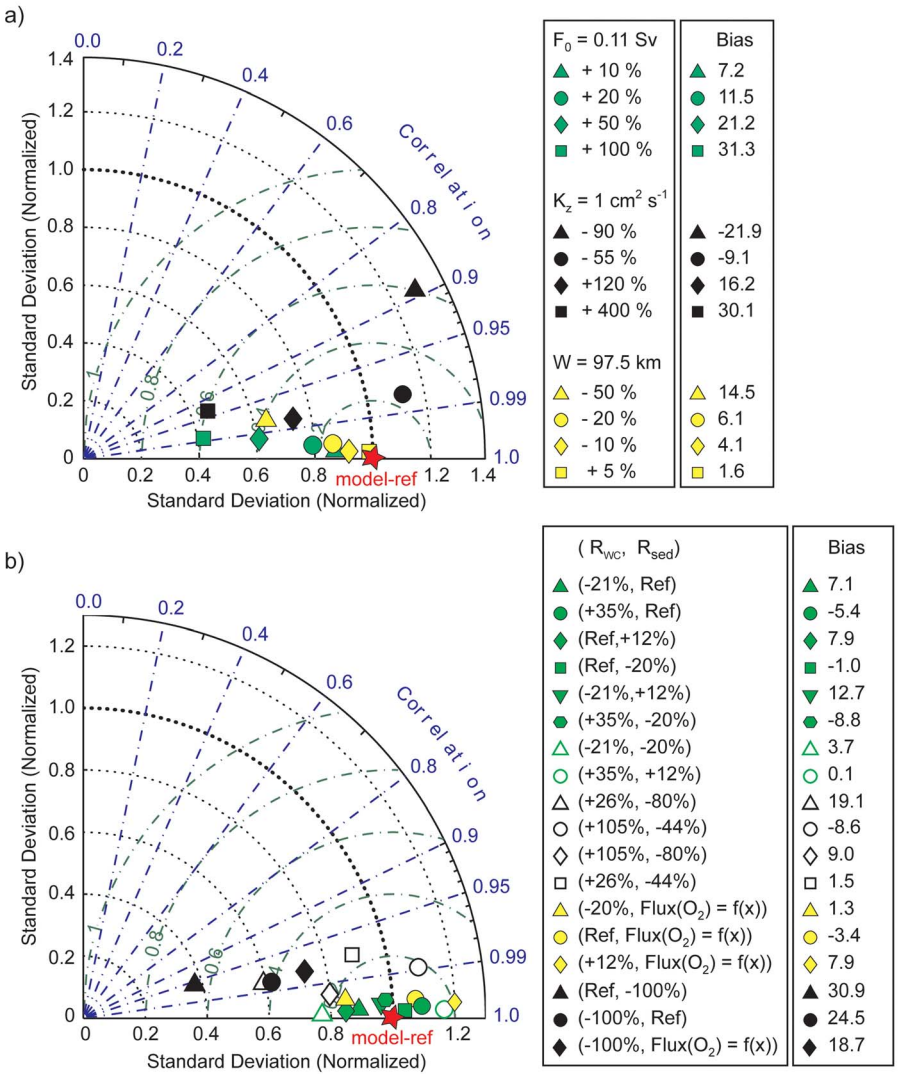

Figure 9. Taylor diagrams for dissolved oxygen concentrations showing results of the sensitivity study to (a) physical parameters and (b) benthic and pelagic respiration rates compared to the reference simulation. The percentages represent deviations from the reference (see Tables 5 and 6 for corresponding values) within the possible ranges of parameters. The bias (M_{model} - M_{data}) is expressed in mmol O_2 m^{-3}. In Figure 9a, the transport variations are represented in green; the vertical diffusion coefficient variations are represented in black; the channel width variations, impacting the horizontal advection velocity (see text for more details), are represented in yellow. Benthic and pelagic respiration rates are fixed to their reference values at −3540 mmol O_2 m^{-2} yr^{-1} and −19.6 mmol O_2 m^{-3} yr^{-1}, respectively. In Figure 9b, the pair of numbers in brackets represents variations of the pelagic and benthic respiration rates from the reference values. Physical parameters are fixed to their reference values: F_0 = 0.11 Sv, W = 97.5 km and K_z = 1 cm^2 s^{-1}. Filled green symbols represent variations of the R_{sed}:R_{wc} ratio from the reference value of 3:2 [*Lehmann et al.*, 2009]; open green symbols represent the maximal and minimal variations of the total respiration at a fixed R_{sed}:R_{wc} ratio of 3:2 [*Lehmann et al.*, 2009]; open black symbols encompass the range of measured values by incubations for benthic respiration and ETS for pelagic respiration; filled yellow symbols represent the sensitivity for an along channel variable benthic respiration (F_{O2} = f(x) defined from the diagenetic model of *Benoit et al.* [2006], the function is plotted on Figure 5); and filled black symbols represent simulations with either pelagic or benthic respiration alone.

[27] Apart from the horizontal diffusion, which makes a small contribution to the oxygen budget regardless of the location along the channel, the transport modes above and below the oxygen minimum change considerably (Figure 10). Above the oxygen minimum, dissolved oxygen is supplied by both vertical diffusion and vertical advection, and is lost by horizontal advection. Below the oxygen minimum, it is the opposite: oxygen is mainly supplied by horizontal advection, while it is lost by vertical diffusion across the sediment-water interface because of benthic respiration and by vertical advection across the oxygen minimum because of an upward vertical advection. Due to the

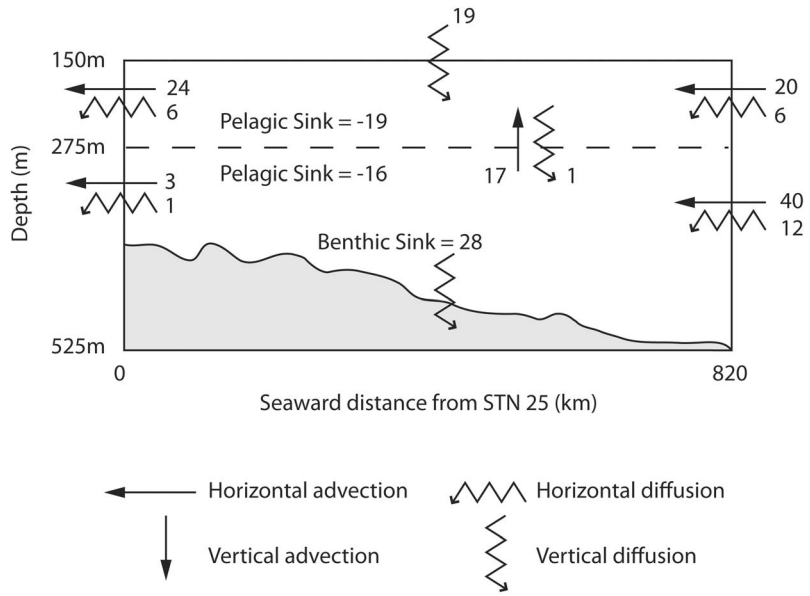

Figure 10. Dissolved oxygen budget in the bottom waters of the Laurentian Channel, separated along the dissolved oxygen minimum at 275 m depth. The dissolved oxygen budget is calculated using the reference simulation parameters. Integrated fluxes are in 10^{10} mol O_2 yr^{-1}. The vertical diffusion at the sediment-water interface was calculated from R_{sed} and integrated over the whole sediment surface area. The error is $\pm 1 \times 10^{10}$ mol O_2 yr^{-1}.

reduction of the water column height from Cabot Strait to Station 25 (Figure 6), the horizontal velocity increases landward and generates a vertical velocity faster near the sediment-water interface than anywhere else in the water column (Table 1, equation (4)). As a consequence, the advection of oxygen coming from the North Atlantic Ocean increases landward and upward which displaces the oxygen minimum from the sediment-water interface into the water column, as reflected by the positive slope of the oxygen concentration isopleths along the Laurentian Channel (in the seaward direction) (Figure 8). Above the oxygen minimum, where oxygen is supplied by both vertical advection and vertical diffusion, oxygen concentration isopleths have a negative slope along the Laurentian Channel (in the seaward direction). Therefore, the balance between vertical advection and vertical diffusion determines the depth of the oxygen minimum. This finding implies that the physics of the system is mostly responsible for the generation of the dissolved oxygen minimum, and probably for its general geographical distribution pattern.

[28] A vertical distribution of dissolved oxygen similar to that observed along the Laurentian Channel has been reported in a coastal upwelling system off Namibia [*Gutknecht et al.*, 2011], where the physical processes are known to control the development and intensification of subsurface oxygen-depleted water [e.g., *Monteiro et al.*, 2008, 2011]. Physical processes can affect the dissolved oxygen concentration through either weak ventilation [*Czeschel et al.*, 2011] or remote advection of oxygen-depleted water masses [*Bograd et al.*, 2008]. Physical processes, such as wind-forcing, can also influence the biogeochemical oxygen demand through the intensification of the upwelling of nutrient-rich water [*Monteiro et al.*, 2006] which promotes primary production [*Mohrholz et al.*, 2008] and, in turn, can lead to eutrophication [*Monteiro and Largier*, 1999]. Although upwelling at the head of the Laurentian Channel is not physically represented in our model, it is an intrinsic part of the St. Lawrence estuarine circulation system and strongly influences primary production in the surface waters of the LSLE, which, in turn, is ultimately exported to the bottom waters and modifies the strength of the pelagic and benthic oxygen sinks. In contrast to coastal upwelling systems, intensification of upwelling at the head of the Laurentian Channel has been mostly observed in winter [*Smith et al.*, 2006] when the temperature, the ice cover and the low light conditions limit phytoplankton growth. Thus, we believe that the establishment of hypoxia in the bottom waters of the LSLE results mostly from the weak ventilation and the low initial dissolved oxygen concentration in the advected water rather than from an intensification of the biogeochemical oxygen demand, as our model reproduces the hypoxia observed in the LSLE (Figure 8) with constant benthic and pelagic respiration rates throughout the Laurentian Channel.

[29] Dissolved oxygen concentrations in the bottom waters of the LSLE have decreased by 50% over the last century [*Gilbert et al.*, 2005]. A concurrent warming of these waters [*Thibodeau et al.*, 2010; *Genovesi et al.*, 2011; *Sherwood et al.*, 2011] suggests that changes in the relative proportions of the cold oxygen-rich LCW and the warm oxygen-poor NACW, whose mixture makes up the bottom waters feeding the Laurentian Channel, modified their properties and played a determining role in the progressive depletion of dissolved oxygen and ultimate establishment of hypoxic conditions in the LSLE [*Gilbert et al.*, 2005]. *Gilbert et al.* [2005] estimated that one half to two thirds of the oxygen loss in the LSLE could be attributed to modifications of the water circulation pattern on the eastern

Canadian continental shelf where LCW and NACW mix, while the remaining third was tentatively ascribed to eutrophication [*Gilbert et al.*, 2005]. Whereas *Thibodeau et al.* [2006] demonstrated, using geochemical and micropaleontological tracers in the sediment, that primary productivity and the flux of marine organic matter to the seafloor might have increased over the last 30–40 years in the LSLE, *Genovesi et al.* [2011], using the same tracers, showed that the organic matter input to the seafloor in the Gulf of St. Lawrence has been nearly constant for the last two centuries while the bottom water dissolved oxygen gradient between Cabot Strait and the LSLE has increased since the turn of the century (∼1880–1910). *Genovesi et al.* [2011] proposed that the nearly 1.7°C increase in temperature of the waters entering the Laurentian Channel and the resulting increased respiration rates may be responsible for the increasing oxygen gradient in the Gulf of St. Lawrence since the early 1930s [*Gilbert et al.*, 2005]. Likewise, our model results suggest that the horizontal advection of water with lower dissolved oxygen concentration is mostly responsible for the establishment of hypoxic conditions in the Lower Estuary. Since climate models predict the expansion of oxygen minimum zones under global warming conditions [*Matear and Hirst*, 2003], the hypoxic zone in the Laurentian Channel may spread from the LSLE to the Gulf. Only long-term monitoring of the LSLE and Gulf of St. Lawrence will allow us to elucidate how the St. Lawrence ecosystem will respond to climate change.

6. Conclusions

[30] This study examined the role of physical and biogeochemical processes and their relative contributions on the spatial distribution of dissolved oxygen in the bottom waters of the Laurentian Channel, using a simple 2-D advection-diffusion model. The inclusion of a realistic bathymetry to an earlier model [*Benoit et al.*, 2006], combined with independently derived benthic and pelagic respiration rates, reproduced the observed geographical distribution of dissolved oxygen concentrations. Spatial changes in the flow velocity of bottom waters, induced by the inclusion of a realistic bathymetry, are mostly responsible for generating the fine-scale vertical distribution pattern of dissolved oxygen and, more importantly, the presence of a mid-water column oxygen minimum, while benthic and pelagic sinks only influence the intensity of the oxygen minimum. Our simulations of bottom water oxygen concentrations and distribution pattern along the Laurentian Channel show that the system is much more sensitive to physical than biogeochemical processes and demonstrate that the oceanographic conditions at the continental shelf edge, where Laurentian Channel bottom waters originate, and the circulation within the Channel are mostly responsible for the establishment of hypoxic conditions in the Lower Estuary.

[31] **Acknowledgments.** This research was funded by a NSERC Strategic grant to A.M., D.G. and Y.G, and a DFO CCSI (Climate Change Science Initiative) grant to D.G. Additional financial support to S.L. was provided by the Department of Earth and Planetary Sciences/McGill, the GEOTOP-UQAM-McGill research center, the LEGOS laboratory and the University of Toulouse III (Paul Sabatier, France). We thank the captains and crew of R/V Alcide C. Horth and R/V Coriolis II for their help during the numerous cruises between 2002 and 2011. We acknowledge the two anonymous reviewers for their insightful comments.

References

Anschutz, P., B. Sundby, L. LeFrançois, G. W. Luther III, and A. Mucci (2000), High resolution profiles and fluxes of redox species in continental margin sediments: Implication for the cycles of nitrogen, iodide, manganese, and iron, *Geochim. Cosmochim. Acta*, *64*, 2751–2763, doi:10.1016/S0016-7037(00)00400-2.

Benoit, P., Y. Gratton, and A. Mucci (2006), Modeling of dissolved oxygen levels in the bottom waters of the Lower St. Lawrence Estuary: Coupling of benthic and pelagic processes, *Mar. Chem.*, *102*, 13–32, doi:10.1016/j.marchem.2005.09.015.

Bograd, S., C. G. Castro, E. Di Lorenzo, D. M. Palacios, H. Bailey, W. Gilly, and F. P. Chavez (2008), Oxygen declines and the shoaling of the hypoxic boundary in the California Current, *Geophys. Res. Lett.*, *35*, L12607, doi:10.1029/2008GL034185.

Bugden, G. L. (1991), Changes in the temperature-salinity characteristics of the deeper waters of the Gulf of St. Lawrence over the past several decades, in *The Gulf of St. Lawrence: Small Sea or Big Estuary?*, edited by J.-C. Therriault, *Can. Spec. Publ. Fish. Aquat. Sci.*, *113*, 139–147.

Chapman, D. C. (1985), Numerical treatment of cross-shelf open boundaries in a barotropic coastal ocean model, *J. Phys. Oceanogr.*, *15*, 1060–1075, doi:10.1175/1520-0485(1985)015<1060:NTOCSO>2.0.CO;2.

Cloern, J. E. (2001), Our evolving conceptual model of the coastal eutrophication problem, *Mar. Ecol. Prog. Ser.*, *210*, 223–253, doi:10.3354/meps210223.

Colombo, J. C., N. Silverberg, and J. N. Gearing (1996a), Biogeochemistry of organic matter in the Laurentian Trough. I. Composition and vertical fluxes of rapidly settling particles, *Mar. Chem.*, *51*, 277–293, doi:10.1016/0304-4203(95)00059-3.

Colombo, J. C., N. Silverberg, and J. N. Gearing (1996b), Biogeochemistry of organic matter in the Laurentian Trough. II. Bulk components during early diagenesis, *Mar. Chem.*, *51*, 295–314, doi:10.1016/0304-4203(95)00060-7.

Craig, J., and D. Gilbert (2008), Estimation of mixed layer depth at the AZMP fixed stations, *AZMP Bull.*, *7*, 37–42.

Czeschel, R., L. Stramma, F. U. Schwarzkopf, B. S. Giese, A. Funk, and J. Karstensen (2011), Mid-depth circulation of the eastern tropical south Pacific and its link to the oxygen minimum zone, *J. Geophys. Res.*, *116*, C01015, doi:10.1029/2010JC006565.

Diaz, R. J. (2001), Overview of hypoxia around the world, *J. Environ. Qual.*, *30*, 275–281, doi:10.2134/jeq2001.302275x.

Diaz, R. J., and D. L. Breitburg (2009), The hypoxic environment, in *Hypoxia in fishes*, edited by J. G. Richards et al., pp. 1–23, Elsevier, San Diego, doi:10.1016/S1546-5098(08)00001-0.

Dickie, L. M., and R. W. Trites (1983), The Gulf of St. Lawrence, in *Estuaries and Enclosed Seas*, edited by B. H. Ketchum, pp. 403–425, Elsevier, Amsterdam.

Galbraith, P. S. (2006), Winter water masses in the Gulf of St. Lawrence, *J. Geophys. Res.*, *111*, C06022, doi:10.1029/2005JC003159.

Genovesi, L., A. de Vernal, B. Thibodeau, C. Hillaire-Marcel, A. Mucci, and D. Gilbert (2011), Recent changes in bottom water oxygenation and temperature in the Gulf of St. Lawrence: Micropaleontological and geochemical evidence, *Limnol. Oceanogr.*, *56*(4), 1319–1329, doi:10.4319/lo.2011.56.4.1319.

Gilbert, D. (2004), Propagation of temperature signals along the north-west Atlantic continental shelf edge and into the Laurentian Channel, paper presented at ICES Annual Science Conference, Int. Counc. for the Explor. of the Sea, Vigo, Spain.

Gilbert, D., and B. Pettigrew (1997), Interannual variability (1948–1994) of the CIL core temperature in the Gulf of St. Lawrence, *Can. J. Fish. Aquat. Sci.*, *54*, 57–67.

Gilbert, D., B. Sundby, C. Gobeil, A. Mucci, and G. H. Tremblay (2005), A seventy-two-year record of diminishing deep-water oxygen in the St. Lawrence Estuary: The northwest Atlantic connection, *Limnol. Oceanogr.*, *50*, 1654–1666, doi:10.4319/lo.2005.50.5.1654.

Gilbert, D., N. N. Rabalais, R. J. Diaz, and J. Zhang (2010), Evidence for greater oxygen decline rates in the coastal ocean than in the open ocean, *Biogeosciences*, *7*, 2283–2296, doi:10.5194/bg-7-2283-2010.

Glud, R. N., J. K. Gundersen, B. B. Jorgensen, N. P. Revsbech, and H. D. Schulz (1994), Diffusive total oxygen uptake of deep-sea sediments in the eastern South Atlantic Ocean: In situ and laboratory measurements, *Deep Sea Res., Part I*, *41*(11–12), 1767–1788, doi:10.1016/0967-0637(94)90072-8.

Grasshoff, K., K. Kremling, and M. Ehrhardt (Eds.) (1999), *Methods of Seawater Analysis*, 3rd ed., Wiley-VCH, Weinheim, Germany, doi:10.1002/9783527613984.

Gratton, Y., G. Mertz, and J. A. Gagné (1988), Satellite observations of tidal upwelling and mixing in the St. Lawrence Estuary, *J. Geophys. Res.*, *93*, 6947–6954, doi:10.1029/JC093iC06p06947.

Gutknecht, E., et al. (2011), Nitrogen transfers and air-sea N_2O fluxes in the upwelling off Namibia within the oxygen minimum zone: A 3-D model approach, *Biogeosci. Discuss.*, *8*, 3537–3618, doi:10.5194/bgd-8-3537-2011.

Han, G., J. W. Loder, and P. C. Smith (1999), Seasonal-mean hydrography and circulation in the Gulf of St. Lawrence and on the eastern Scotian and southern Newfoundland shelves, *J. Phys. Oceanogr.*, *29*, 1279–1301, doi:10.1175/1520-0485(1999)029<1279:SMHACI>2.0.CO;2.

Johnson, C. (1987), *Numerical Solution of Partial Differential Equations by the Finite Element Method*, Studentlitteratur, Lund, Sweden.

Katsev, S., G. Chaillou, B. Sundby, and A. Mucci (2007), Effects of progressive oxygen depletion on sediment diagenesis and fluxes: A model for the Lower St. Lawrence River Estuary, *Limnol. Oceanogr.*, *52*(6), 2555–2568, doi:10.4319/lo.2007.52.6.2555.

Koutitonsky, V. G., and G. L. Bugden (1991), The physical oceanography of the Gulf of St. Lawrence: A review with emphasis on the synoptic variability of the motion, in *The Gulf of St. Lawrence: Small Sea or Big Estuary?*, edited by J.-C. Therriault, *Can. Spec. Publ. Fish. Aquat. Sci.*, *113*, 139–147.

Large, W. G., J. C. McWilliams, and S. C. Doney (1994), Oceanic vertical mixing: A review and a model with nonlocal boundary layer parameterization, *Rev. Geophys.*, *32*(4), 363–403, doi:10.1029/94RG01872.

LeBlond, P. H., and L. A. Mysak (1978), *Waves in the Ocean*, Elsevier, New York.

Ledwell, J. R., A. J. Wilson, and C. S. Low (1993), Evidence for slow mixing across the pycnocline from an open-ocean tracer-release experiment, *Nature*, *364*, 701–703, doi:10.1038/364701a0.

Lehmann, M. F., B. Barnett, Y. Gélinas, D. Gilbert, R. J. Maranger, A. Mucci, B. Sundby, and B. Thibodeau (2009), Aerobic respiration and hypoxia in the Lower St. Lawrence Estuary: Stable isotope ratios of dissolved oxygen constrain oxygen sink partitioning, *Limnol. Oceanogr.*, *54*(6), 2157–2169, doi:10.4319/lo.2009.54.6.2157.

Lucotte, M., C. Hillaire-Marcel, and P. Louchouarn (1991), First-order organic carbon budget in the St. Lawrence Lower Estuary from ^{13}C data, *Estuarine Coastal Shelf Sci.*, *32*, 297–312, doi:10.1016/0272-7714(91)90022-4.

Matear, R. J., and A. C. Hirst (2003), Long-term changes in dissolved oxygen concentrations in the ocean caused by protracted global warming, *Global Biogeochem. Cycles*, *17*(4), 1125, doi:10.1029/2002GB001997.

Mathworks, Inc. (2006), Partial Differential Equation Toolbox–User's guide, Natick, Mass.

Mohrholz, V., C. H. Bartholomae, A. K. van der Plas, and H. U. Lass (2008), The seasonal variability of the northern Benguela undercurrent and its relation to the oxygen budget on the shelf, *Cont. Shelf Res.*, *28*, 424–441, doi:10.1016/j.csr.2007.10.001.

Monteiro, P. M. S., and J. L. Largier (1999), Thermal stratification in Saldanha Bay (South Africa) and subtidal, density-driven exchange with the coastal waters of the Benguela upwelling system, *Estuarine Coastal Shelf Sci.*, *49*(6), 877–890, doi:10.1006/ecss.1999.0550.

Monteiro, P. M. S., A. van der Plas, V. Mohrholz, E. Mabille, A. Pascall, and W. Joubert (2006), Variability of natural hypoxia and methane in a coastal upwelling system: Oceanic physics or shelf biology?, *Geophys. Res. Lett.*, *33*, L16614, doi:10.1029/2006GL026234.

Monteiro, P. M. S., A. van der Plas, J.-L. Mélice, and P. Florenchie (2008), Interannual hypoxia variability in a coastal upwelling system: Ocean-shelf exchange, climate and ecosystem-state implications, *Deep Sea Res., Part I*, *55*, 435–450, doi:10.1016/j.dsr.2007.12.010.

Monteiro, P. M. S., B. Dewitte, M. I. Scranton, A. Paulmier and A. van der Plas (2011), The role of open ocean boundary forcing on seasonal to decadal-scale variability and long-term change of natural shelf hypoxia, *Environ. Res. Lett.*, *6*, 025002, doi:10.1088/1748-9326/6/2/025002.

Muzuka, A. N. N., and C. Hillaire-Marcel (1999), Burial rates of organic matter along the eastern Canadian margin and stable isotope constraints on its origin and diagenetic evolution, *Mar. Geol.*, *160*, 251–270, doi:10.1016/S0025-3227(99)00022-5.

Özsoy, E., and Ü. Ünlüata (1997), Oceanography of the Black Sea: A review of some recent results, *Earth Sci. Rev.*, *42*, 231–272, doi:10.1016/S0012-8252(97)81859-4.

Packard, T. T. (1985), Measurement of electron transport activity of microplankton, *Adv. Aquat. Microbiol.*, *3*, 207–261.

Peña, M. A., S. Katsev, T. Oguz, and D. Gilbert (2010), Modeling dissolved oxygen dynamics and hypoxia, *Biogeosciences*, *7*, 933–957, doi:10.5194/bg-7-933-2010.

Saucier, F. J., F. Roy, D. Gilbert, P. Pellerin, and H. Ritchie (2003), Modeling the formation and circulation processes of water masses and sea ice in the Gulf of St. Lawrence, Canada, *J. Geophys. Res.*, *108*(C8), 3269, doi:10.1029/2000JC000686.

Savenkoff, C., A. F. Vézina, J.-P. Chanut, and Y. Gratton (1995), Respiratory activity and CO_2 production rates of microorganisms in the Lower St. Lawrence Estuary, *Cont. Shelf Res.*, *15*(6), 613–631, doi:10.1016/0278-4343(94)00041-K.

Savenkoff, C., et al. (1996), Distributions of oxygen, carbon, and respiratory activity in the deep layer of the Gulf of St. Lawrence and their implications for the carbon cycle, *Can. J. Fish. Aquat. Sci.*, *53*, 2451–2465, doi:10.1139/f96-198.

Savenkoff, C., A. F. Vézina, P. C. Smith, and G. Han (2001), Summer transports of nutrients in the Gulf of St. Lawrence estimated by inverse modeling, *Estuarine Coastal Shelf Sci.*, *52*, 565–587, doi:10.1006/ecss.2001.0774.

Sherwood, O. A., M. F. Lehmann, C. J. Schubert, D. B. Scott, and M. D. McCarthy (2011), Nutrient regime shift in the western North Atlantic indicated by compound-specific $\delta^{15}N$ of deep-sea gorgonian corals, *Proc. Natl. Acad. Sci. U. S. A.*, *108*, 1011–1015, doi:10.1073/pnas.1004904108.

Silverberg, N., B. Sundby, A. Mucci, S. Zhong, T. Arakaki, P. Per Hall, A. Landén, and A. Tengberg (2000), Remineralization of organic carbon in eastern Canadian continental margin sediments, *Deep Sea Res., Part I*, *47*, 699–731.

Smith, G. C., F. J. Saucier, and D. Straub (2006), Response of the Lower St. Lawrence Estuary to external forcing in winter, *J. Phys. Oceanogr.*, *36*, 1485–1501, doi:10.1175/JPO2927.1.

Smith, J. N., and C. T. Schafer (1999), Sedimentation, bioturbation, and Hg uptake in the sediments of the Estuary and Gulf of St. Lawrence, *Limnol. Oceanogr.*, *44*, 207–219, doi:10.4319/lo.1999.44.1.0207.

Taylor, K. E. (2001), Summarizing multiple aspects of model performance in a single diagram, *J. Geophys. Res.*, *106*, 7183–7192, doi:10.1029/2000JD900719.

Tee, K.-T. (1989), Subtidal salinity and velocity variations in the St. Lawrence Estuary, *J. Geophys. Res.*, *94*, 8075–8090, doi:10.1029/JC094iC06p08075.

Thibodeau, B., A. de Vernal, and A. Mucci (2006), Recent eutrophication and consequent hypoxia in the bottom waters of the Lower St. Lawrence Estuary: Micropaleontological and geochemical evidence, *Mar. Geol.*, *231*, 37–50, doi:10.1016/j.margeo.2006.05.010.

Thibodeau, B., A. De Vernal, C. Hillaire-Marcel, and A. Mucci (2010), Twentieth century warming in deep waters of the Gulf of St. Lawrence: A unique feature of the last millennium, *Geophys. Res. Lett.*, *37*, L17604, doi:10.1029/2010GL044771.

Vosjan, J. H., and G. Nieuwland (1987), Microbial biomass and respiratory activity in surface waters of the East Banda Sea and North West Arafura Sea (Indonesia) at the time of the South East Monsoon, *Limnol. Oceanogr.*, *32*, 767–775, doi:10.4319/lo.1987.32.3.0767.

Vosjan, J. H., S. B. Tijssen, G. Nieuwland, and F. J. Wetsteyn (1990), Oxygen regime, respiratory activity and biomass of microorganisms, and the carbon budget in the Fladen Ground area (Northern North Sea) during spring, *Neth. J. Sea Res.*, *25*, 89–99, doi:10.1016/0077-7579(90)90011-5.